IZMIR UNIVERSITY OF ECONOMICS

FACULTY OF ENGINEERING

AEROSPACE ENGINEERING

Trajectory Design and Flight Dynamics of a Solar-Sail Propelled CubeSat Class Spacecraft Targeting Mars and its Moons

Authors: Ceren Zengin

Can Oral

İdris Emre Özer

Tolga Turhan

Supervisor: Dr. Fabrizio Pinto

https://doi.org/10.5281/zenodo.8191968

We would like to sincerely thank our supervisor Dr. Fabrizio Pinto for his guidance and continuous help throughout this project.

Contents

FENG 498
Final Report
Trajectory design and flight dynamics of a solar-sail propelled CubeSat class spacecraft targeting Mars and its moons

Ceren Zengin, Can Oral, İdris Emre Özer, Tolga Turhan

July 28, 2023

Abstract

Solar radiation pressure is a very significant aspect of any space mission, both in terms of perturbations and propagation, such as in the case of solar sailing. Because traditional spacecraft consume considerable amounts of fuel and are expensive, there has been an increase in interest in solar sails, which is an affordable and easier way to navigate through space, using only the momentum of photons from the Sun. This study aims to further develop the mission designed to reach Mars with a solar sail powered CubeSat spacecraft. To make the mission as realistic as possible, detailed orbital analyses of several Mars orbiter missions are performed and the orbiters are implemented into the script, as well as the moons of Mars, Phobos and Deimos. Additionally, the orbital design and analysis necessary to make it possible to fly by Mars and the Martian moons are performed. The analyses carried out in this study highlighted the advantages of solar sailing, showing the possibility of an interplanetary mission without chemical engines. A more accurate model of solar radiation pressure is implemented with the use of a SPAD file, allowing us to observe the differences in SRP models. The cannonball model is implemented in this study for a more realistic approach to solar radiation pressure. Furthermore, several FOSS software, such as GMAT, Horizons and Mathematica are used for analyses, plotting and simulations, which are discussed in detail. This study aims to act as a guide for future interplanetary solar sail powered missions.

List of Symbols, Abbreviations and Definitions

aerobrake The technique used to decrease the orbital energy of the spacecraft, by using the atmospheric drag of the celestial body. 31, 33

AOP Argument of periapsis, the angle between the direction of the periapsis and the direction of the ascending node, measured in the plane of the orbit. 11, 41

apoapsis The location in an orbit where the orbiting object is furthest away from the parent celestial body. If the orbit is around the Sun, specified as aphelion. 11, 24, 27, 34

AstroGrav A Free open-source software for space and solar system simulations. 10, 37

AU Astronomical Unit: average distance between the Earth and the Sun, approximately 150 million kilometers. 12

CubeSat A miniaturized and light satellite class used for space exploration which is consisted of cubic modules. 5, 9, 15, 16

Deep Space Network A worldwide network of spacecraft communication ground segment facilities, located in the United States, Spain, and Australia, which supports interplanetary spacecraft missions. 16

ECC Eccentricity, the measure of the deviation of an ellipse from being circular, with values ranging from 0 (a circle) to greater than 1 (hyperbolic trajectory), denoted with "e". 11, 27, 33, 35, 39, 41

Epoch Epoch is a specific point in time used as a reference for the measurement of celestial positions. It is often used in conjunction with orbital elements, which are only valid for a specific epoch. 22, 29

FOSS Free Open Source Software, open-source software that is freely licensed to use. 10

FOV Field of View, the maximum area that can be covered by a camera. 25

GMAT General Mission Analysis Tool, NASA 9, 10, 14, 15, 17, 18, 22, 26, 27, 35, 37, 39–42

Gnuplot A free open-source software for mathematical analysis and plotting. 34

Horizons System A web-based system by the Jet Propulsion Laboratory which allows the user to obtain the orbital elements and position of any known body in the Solar System. 10, 21–23, 29, 31–33, 41

INC Inclination, the angle between an object's orbit plane and a reference plane, usually the plane of the celestial equator or the ecliptic plane. 11, 41

JPL Jet Propulsion Laboratory, NASA 21, 31, 32

Jupyter Notebook An interactive, web base computing platform that allows many kernels from different softwares. 35

JWST James Webb Space Telescope 12

k_{eff} Effective standard gravitational parameter. 27

$L_{\odot}$ Luminosity of the Sun. 26, 27

Libration points Points in space where the gravitational effects of two massive bodies create an equilibrium. Also known as Lagrange Points 12

MarsFixed The reference frame in GMAT that centers the centroid of Mars. 34, 35

Mathematica A mathematical software that is mainly used for technical computing, plotting and statistical analysis. 35

MAVEN Mars Atmosphere and Volatile Evolution, NASA 3, 10–12, 21, 22, 24, 29, 31, 34, 36, 41

MEO Medium Earth Orbit is an Earth-centered orbit, with altitudes between 2000 and 35786 kilometers. 39

MEX Mars Express, ESA 10, 21, 22, 24, 31, 32, 36, 41

$\hat{\mathbf{n}}$ Normal unit vector of the solar sail 12

NASA National Aeronautics and Space Administration 9, 14, 16, 17, 31, 33

On-Off The maneuver performed autonomously by the spacecraft that allows it to maximize the energy gained traveling away from the Sun and minimize the energy lost traveling towards the Sun. 9

OSIRIS-Rex Origins, Spectral Interpretation, Resource Identification, Security, Regolith Explorer (OSIRIS-Rex) is NASA's asteroid research and sample return mission Which is aimed to obtain samples from asteroid Bennu 14, 15

periapsis The location in an orbit where the orbiting object is closest to the parent celestial body. If the orbit is around the Sun, specified as perihelion. 11, 24, 31, 33

RAAN Right ascension of the ascending node (also called the longitude of the ascending node), the angle between the reference plane and the point where the orbit of an object crosses the reference plane moving northward. 41

SMA Semi-Major Axis, a measure of the size of an ellipse, specifically the distance from the center to the apoapsis, denoted with "a". 27, 39, 41

SOI Sphere of Influence, the area where the main gravitational force is due to the parent body, and other forces can be neglected. 24

Solar Radiation Pressure The pressure exerted by photons, thus inversely proportional with distance to the Sun. 9, 11–15, 17, 24, 32, 39, 40

solar-sail A technique implemented to spacecraft that allows propagation through the momentum of photons. 3, 5, 9–12, 15, 16, 22, 24, 26, 28, 29, 33, 41

SPAD Solar Pressure and Aerodynamic Drag Tool 10, 14, 15, 39–42

TA True anomaly, the angle between the direction of an object in its orbit and the direction of the periapsis, measured in the plane of the orbit. 41

$\boldsymbol{v}$ velocity 27, 28

$\hbar$ Planck constant 10

Δv Change in velocity 16, 33

η Solar sail efficiency (Coefficient of Reflectivity in GMAT). 13, 26, 28

λ Wavelength 10

σ Area-to-mass ratio of the spacecraft. 12, 13

1 Introduction

The number of missions to Mars is rising each year, especially with the growing demand for space tourism and exploration. While there are many engine-powered missions both succeeded or were planned, the use of solar-sails is growing in popularity in the space industry. There are many significant benefits of solar-sailing, to give some examples, they are incredibly cheaper to both operate and produce, they are considerably smaller, as they operate with mostly CubeSats, and most importantly, relying on "the heavenly breezes" as Johannes Kepler stated in 1619 [1], solar-sailing eliminates all use of fuel, therefore they are incredibly light compared to conventional spacecraft.

This mission makes use of only solar-sails, without any engine on board, on an interplanetary trajectory, which has never been done before. The case of this study is completely designed in NASA's GMAT programme, where the orbit of the spacecraft is determined by 6 orbital elements, as well as the mass and the area of Solar Radiation Pressure. The spacecraft begins its mission, with an orbit around the Sun, initially moving towards its first aphelion and perihelion. According to the position of the spacecraft with respect to the Sun, On-Off maneuvering is implemented, allowing the spacecraft to gain orbital energy when moving away from the Sun in the "On" position, and contrarily avoid (or minimize) losing energy while propagating towards the Sun, in the "Off" position [2].

The paper begins by examining some of the pioneering work that guided the team in this study, in Sec. 2, continued with Sec. 3 where the methodology of using some of the programmes. In Sec. 4, the obtained results are discussed and analyzed, and the report is concluded with Sec. 5.

1.0.1 Momentum of a Photon

Since photons are massless particles by nature, it is impossible to calculate their momentum with the regular formula $p = mv$. Instead, the momentum of a photon comes from the Special Theory of Relativity by Einstein and the Dirac Equation. From relativistic quantum theory, the conservation of the energy-momentum equation is as below [3];

$$E^2 - p^2 = m^2 \tag{1}$$

This equation gives the relation between energy and momentum in standard particle physics, where the speed of light is taken as 1. From the Special Theory of Relativity, including the speed of light, $E^2 = (mc^2)^2 + (pc)^2$. Deriving the equation for momentum;

$$p = \sqrt{\frac{E^2}{c^2} - m^2c^2} \tag{2}$$

For the case of a photon, substituting $m = 0$, $p = \frac{E}{c}$. Then applying the equation $E = \frac{hc}{\lambda}$, we get the relation giving the momentum of a photon with respect to the Planck constant and wavelength;

$$p = \frac{\hbar c}{c\lambda} = \frac{\hbar}{\lambda} \tag{3}$$

1.1 Problem Statement

The main aim of this study was to develop and improve what was learned from the first part of this mission. The simulation is altered in many ways to plan and execute a mission that is more realistic and more detailed. To achieve more realistic results, 3 orbiters of Mars (MEX, MAVEN and Mars Odyssey) are manually implemented in the system, as well as the moons of Mars, Phobos and Deimos. This improvement allowed the mission to possibly include flybys to the moons of the red planet. By analyzing the orbits of the three operating spacecraft around Mars, the trajectory of the main spacecraft is altered when needed, to avoid any collision. Additionally, SPAD files are experimented with, on a separate mission to further develop the use of solar radiation pressure. With these additions to the initial mission, this study aims to provide some information for future work regarding interplanetary solar-sailed spacecraft missions.

1.2 Motivation

As well as designing a low-thrust mission to Mars and its moons, this study aims to be a guide for future missions operating on solar radiation pressure. SPAD files are a subject that is difficult to find references to, therefore it is a goal of this paper to include a simplified and summarized version of the cannonball approximation. Continuing, the importance of crash avoidance in interplanetary missions is highlighted in this study, with the implementation of MEX, MAVEN and Mars Odyssey. The mission is designed to include a flyby to Phobos, therefore allowing us to study the atmosphere and surface of the larger moon. Many different software and programmes are used in this project, such as the Horizons System, GMAT and AstroGrav. Every software and programme are examples of FOSS, hence the mission is designed with a more accessible approach.

The number of missions including a solar-sailed spacecraft will drastically increase in the following years. With the advantages mentioned above, as well as having the possibility to travel up to 9 times the orbital speed of the Space Shuttle

[1], only by the use of Solar Radiation Pressure, solar-sailing is an important concept to study. This paper aims to contribute to the increase in popularity of the solar-sails.

2 Literature Review

2.1 D. C. Folta, "Mars Atmosphere and Volatile Evolution (MAVEN) Mission Design" (2010)

The paper discusses the design and objectives of the Mars Atmosphere and Volatile Evolution (MAVEN) mission, which is the second in the low-cost Mars Scout mission series. The mission aims to determine the role that the loss of volatiles to space has played through time from a highly inclined and high ECC orbit. The launch period is November 18, 2013, with arrival on September 16, 2014. The mission will be conducted from a highly inclined elliptical orbit, which will allow measurements to be made at all altitudes throughout the upper atmosphere, at all local times with respect to the Sun, and at most latitudes. The primary mission will last one Earth year, providing sufficient time to make the key measurements to address the science objectives. The nominal science will be conducted in a 4.5-hour period, 75-degree INC orbit, with a -150 kilometer periapsis altitude. The periapsis altitude will be maintained relative to a density corridor rather than an altitude since the areodetic altitude varies due to the orbital ECC and the oblateness of Mars. The AOP rotates at a rate of -0.808 deg per day, and the Nodal rate is -0.629 deg per day, which will permit science collection over a wide range of periapsis locations. The mission also executes "Deep Dip" campaigns, with periapsis at an altitude near 125 kilometers. This will allow for more detailed measurements of the Martian atmosphere at lower altitudes. MAVEN makes three different types of measurements to achieve its science goals. First, it determines the present-day composition and structure of the upper atmosphere. Second, it determines the present-day escape rate of gas from the upper atmosphere to space. Third, it makes measurements that allow us to extrapolate this escape rate to past times when the solar wind and the solar ultraviolet light were greater to estimate the total amount of gas that has been lost. The paper also discusses the different atmospheric loss and energy processes that MAVEN will measure, including neutral processes shown in blue, ion and plasma processes in red, and solar energetic processes. In brief; the orbit requirements of the MAVEN mission involve maintaining a low periapsis near 150 km while also having an apoapsis greater than 6000 km. This is necessary to meet a density corridor, which refers to a specific range of atmospheric density that the spacecraft must pass through to achieve its scientific goals. The atmosphere of Mars is

highly variable, which makes achieving this requirement challenging. However, the mission design has shown that it is achievable.

2.2 A. Puig, et al. "High-Fidelity Modeling and Visualizing of Solar Radiation Pressure: A Framework for High-Fidelity Analysis" (2019)

Puig and colleagues discuss the importance of Solar Radiation Pressure and how crucial it is for trajectory design, orbit determination and maneuver planning. Although Solar Radiation Pressure is a small perturbation, the study mentions, it has a significant role in many modern missions. It is stated that for spacecraft placed in Libration points, for example, JWST and the Roman Space Telescope, as a result of their high σ, Solar Radiation Pressure is the fourth most significant perturbation after the gravitational effects of the Earth, Moon and the Sun. Puig et al. state that in interplanetary missions such as MAVEN, "(missions that) have large solar panels, accurate modeling of Solar Radiation Pressure improves OD (Orbit Determination) errors and mission plans [4]. For orbiters in missions around small bodies, such as OSIRIX-REX, Solar Radiation Pressure may be as significant as the second most dominant force.

The aim of the study is to develop an open-source framework to compute a high-fidelity model for acceleration due to Solar Radiation Pressure. The program implements 4 different models; cannonball, N-plate, raycast and rayrtace, increasing in fidelity. The high-fidelity models require significantly more computational time and processing, whereas the cannonball and N-plate approximations are easier to compute. The force due to Solar Radiation Pressure on an object with a distance R from the Sun is given by,

$$P_{srp} = \frac{P_0 R_0^2}{cR^2} \tag{4}$$

where P_0 is the solar flux at 1 AU (equals to 1367 W/m^2), R_0 is the mean distance between the Earth and the Sun, and c is the speed of light.

Considering a flat surface such as a solar-sail, the total exerted force by Solar Radiation Pressure is the total of three separate forces. These are from absorbed photons (F_a), reflected photons with (a) specular reflection (F_s) and (b) diffusive reflection (F_d). The forces caused by these cases in the direction $\hat{\mathbf{n}}$ are given by;

$$\vec{F}_a = P_{srp} A \langle \vec{n}, \vec{r}_s \rangle \vec{r}_s \tag{5}$$

$$\vec{F}_s = 2 P_{srp} A \langle \vec{n}, \vec{r}_s \rangle^2 n \tag{6}$$

$$\vec{F}_d = P_{srp} A \langle \vec{n}, \vec{r}_s \rangle (\vec{r}_s + \tfrac{2}{3}\vec{n}) \tag{7}$$

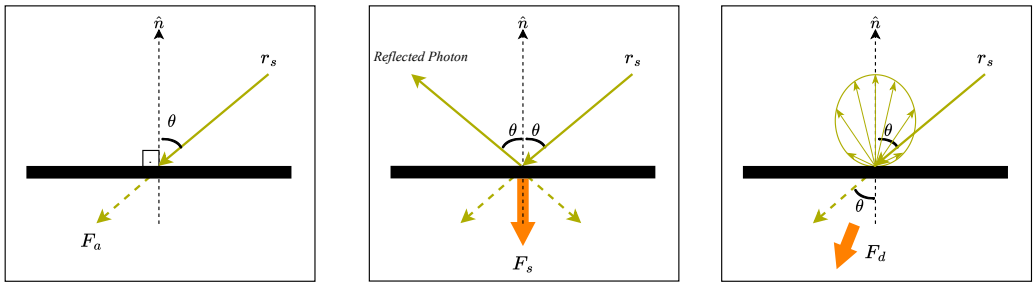

(a) Absorbed Radiation (b) Specular Reflection (c) Diffusive Refleciton

Figure 1: Force due to Solar Radiation Pressure on a flat surface (Adapted from [4], sketched via draw.io)

Puig and colleagues state that the rates of absorption, specular and diffusive reflections are denoted with ρ_a, ρ_s and ρ_d, where $\rho_a + \rho_s + \rho_d = 1$ [4]. From the rates of absorption and reflection, the total force exerted due to Solar Radiation Pressure is given by the equation below.

$$\vec{F_{srp}} = P_{srp} A \langle \vec{n}, \vec{r_s} \rangle \left[(1 - \rho_s)\vec{r_s} + 2\left(\rho_s \langle \vec{n}, \vec{r_s} \rangle + \frac{\rho_d}{3} \right) \vec{n} \right] \tag{8}$$

The simplest way to have a Solar Radiation Pressure model is the cannonball approximation. This method is most commonly used in preliminary mission analysis, due to the low needed computational time. The cannonball model yields the first-order approximation, therefore it is less accurate than the other methods discussed in this study. In this model, Solar Radiation Pressure acceleration is assumed constant throughout the spacecraft, along the direction $\vec{r_s}$, where the acceleration is directly proportional to the area, pressure and η, and inversely proportional to the mass of the spacecraft. σ is an important parameter for the cannonball model since the acceleration decreases as the mass of the spacecraft increases. The coefficient of reflectivity is taken as constant along the surface of the sphere, which is modeled instead of the actual spacecraft. The acceleration due to Solar Radiation Pressure for the cannonball model is given below;

$$\vec{a_{srp}} = \frac{P_{srp} C_r A}{m_{sc}} \vec{r_s} \tag{9}$$

where C_r is the coefficient of reflectivity, (denoted as η in this study), A is the area of the sphere and m_{sc} is the mass of the spacecraft.

The N-plate model is a more accurate approximation than the cannonball model, therefore resulting in more computational time. In this method, the spacecraft is modeled as a collection of multiple flat plates, where their reflectivities are not the same. N-plate approximation allows the force due to Solar Radiation

Pressure to be dependent on the orientation of each surface, therefore dependent on illumination and altitude.

2.3 T. Williams, et al. "Orbit Stability of Osiris-Rex in the Vicinity of Bennu Using a High-Fidelity Solar Radiation Model" (2016)

In this work, it was examined how solar radiation forces affect the trajectory of the Origins Spectral Interpretation Resource Identification Security Regolith Explorer (OSIRIS-Rex) in a high-fidelity model. OSIRIS-Rex is a sample return mission to the asteroid Bennu, a close asteroid to Earth. The mission is a part of NASA's New Frontiers Program. The OSIRIS-Rex spacecraft enters an orbit around Bennu around 3.5 years after launch and stays there for about 60 days. Orbit B is the seventh phase of the mission and is critical to sample recovery success. The primary mission of OSIRIS-Rex during Orbit B is to acquire optical data at 5 cm resolution for 12 prospective touch-and-go sample collection locations, as well as to undertake high-fidelity mapping of Bennu's gravitational field. The nominal Orbit B trajectory is a near circular 1km orbit around Bennu with a period of roughly 27 days, with the orbit normal parallel to the Bennu-Sun direction [5].

In smaller bodies like the asteroids, the effects of the orbital perturbations are much higher for a spacecraft. So, in order to understand these effects combined with the Solar Radiation Pressure forces, a method to accurately model and capture these perturbations has been investigated in this paper. One of these methods in this study was Ray Tracing. The method of tracking the course of a light beam as it absorbs and reflects off various surfaces on the spacecraft is known as ray tracing. Reflected light beams can travel on to encounter many additional surfaces, resulting in further reflections and possibly more future contacts. For computing Solar Radiation Pressure in the SPAD file with the ray tracing algorithm, a simple model of the spacecraft has been done first. Then a plane is generated in space with its normal vector pointing at the origin of the spacecraft's fixed frame body. This normal vector describes the direction in which light from the Sun is emitted onto the spacecraft. The Sun direction, S, is provided by the normal vector of the plane. In the spacecraft's body fixed frame, the S vector, and hence the plane's orientation, may be determined by a given azimuth and elevation angle. The plane's size, which is split into square grids of pixels, is selected to include the whole spaceship. The vector at each pixel's center represents a light ray and is part of the light ray concept. Each light ray model is made up of the vector location and direction, as well as the pixel area. After that, a validation of the SPAD Solar Radiation Pressure force computation has been done using GMAT 2014a version in this paper to simulate OSIRIS-Rex trajectory during Orbit B. Two Solar

Radiation Pressure models have been considered; one is from a cannonball model and one is from SPAD.

In the simulations that used both the Cannonball Solar Radiation Pressure model and the high-fidelity Solar Radiation Pressure model from SPAD, stability of the modified Orbit B has been tested using GMAT. As a result, a much more stable orbit has been achieved in the redesigned Solar Radiation Pressure stable orbit while in the nominal Orbit B trajectory, higher perturbations and lesser stable orbits have been observed. The magnitude of eccentricity variation for the modified Orbit B was lowered to around one-fifth of its nominal value. In conclusion, understanding the trajectory disturbances caused by Solar Radiation Pressure is critical for OSIRIS-Rex's mission success for this paper. By adjusting the eccentricity of the spacecraft's orbit around Bennu, the resultant trajectory remains significantly closer to the nominal terminator orbit in the future.

2.4 T. R. Lockett, et al. "Near-Earth Asteroid Scout Flight Mission" (2019)

The Near Earth Asteroid (NEA) scout is a mission to explore a near-earth asteroid named VG 1991 using a low-thrust solar-sail propulsion system, with an extremely small and inexpensive spacecraft. A 6U CubeSat-based spacecraft will use an 86 m^2 solar-sail that will be used by an NEA Scout. And it will carry a camera, cold gas system, and a full avionics package on an NEA's slow flyby for two years after launch. Since each "U" contains about one liter of volume, the dimensions of a 6U cube are 11 x 24 x 36 cm. The creation of a capability that can bridge strategic knowledge gaps (SKG) at an NEA designated as a human exploration target by the Human Exploration and Operations Mission Directorate (HEOMD) is the mission's success criterion. The sail's low-thrust propulsion will give the CubeSat two key advantages that will allow it to nearly equal the target's velocity. Lockett and colleagues state that a modest relative velocity to the target will make it easier to get ready for a near flyby at the closest approach of less than 1 km and a prolonged operation period close to the target [6]. Strict requirements on spatial resolution and observations under variable illumination necessitate these flyby features. Future surveillance flights will be made possible by this CubeSat's first use as a precursor mission. The spacecraft's architecture adopts the CubeSat design philosophy and methodology, which emphasizes high risk, minimal expense, and a flexible timeline. On its initial mission, known as Artemis 1, NASA's space launch system (SLS) will set the NEA Scout on an Earth escape trajectory. NEA Scout is one of 13 CubeSats that will be released one at a time from the SLS's Orion Stage Adapter after the rocket's primary payload, NASA's Orion crew capsule, is launched on a course for the moon. To maximize power

generation and permit two-way contact with Earth, the spacecraft will be stumbled, stabilized, and pointed toward the sun after ejection using an NEA Scout cold gas thruster. The solar-sail will deploy after the cold gas thrusters have provided an initial Δv capability to target a lunar flyby. NASA's Deep Space Network will be the main ground system for communications and tracking throughout the NEA Scout mission. The first interplanetary CubeSat to image and characterize an NEA smaller than 100 m will be the NEA Scout. Its goal is to fill up strategic knowledge gaps that apply to every astronomical object in this particular class range. The NEA Scout program paves the foundation for the multi-spacecraft study of the NEAs by combining asteroid detection/tracking and proximity science capabilities. The 86 m^2 solar-sail that will be deployed by the NEA Scout will enable the craft to go to an NEA primarily using solar power. Future robotic missions will be able to use NEA Scout to demonstrate low-cost reconnaissance capabilities through the deployment of the sail and navigation to their objective. The scientific advancements made by the NEA Scout include an entire demonstration of onboard image processing as well as science data extraction and prioritization, which can enable missions with limited resources in the future, like trips to the outer solar system. An NEA Scout will be equipped with an Iris X-band radio transponder and a 0.5U camera for autonomous imaging processing. The mission will pave the way for upcoming solar-sail technology demonstration missions and aid in lowering operational costs for CubeSat/SmallSat projects in the future.

2.5 L. G. Jacchia "Solar Effects on the Acceleration of Artificial Satellites" (1963)

The investigation presented here examines the connection between satellite accelerations and sunspot numbers while analyzing the nature of radiation interacting with the upper atmosphere. This paper reveals that fluctuating solar radiation gives rise to atmospheric disturbances which affect global satellite accelerations. As the satellite's perigee height increased, the fluctuations' amplitude also increased. They made up about 20% of the acceleration of Satellite 1958 (perigee height 200 km) in typical, clearly defined 27-day cycles, but 70% of the acceleration in comparable cycles of Satellite 1958 [7]. Additionally, it supplies comprehensive observations alongside an in-depth examination involving diverse satellite traits such as periods of revolution and secular acceleration. All told, the paper strives towards elucidating more fully how solar effects impact not only Earth's atmosphere but also artificial satellites. In summary, fluctuations correspond to the solar flux rhythm at 2800 me (10.7 em wavelength). When the perigee is in darkness, these fluctuations become smaller or vanish while increasing in amplitude with height. These fluctuations most likely represent changes in

atmospheric density brought on by variable short-wave solar radiation (ultraviolet). Magnetic storms are accompanied by brief fluctuations. These alterations appear to be corpuscular in nature and should be interpreted as atmospheric heating caused by some sort of interaction with corpuscular radiation.

2.6 M. Jah, et al. "The General Mission Analysis Tool (GMAT): A New Resource for Supporting Debris Orbit Determination, Tracking and Analysis" (2009)

In this study, the usage of General Mission Analysis Tool (GMAT) in the field of debris orbit determination, and tracking analysis has been discussed with the explanation of GMAT as well. GMAT is developed in the aim of optimizing space trajectories of the spacecraft and celestial bodies and a mission analysis system created in the spirit of the NASA Vision by NASA and commercial sector. The ?? processing architecture inherently allows parallel processing, allowing it to quickly accommodate the orbit determination and monitoring of many breakup objects. This paper talks about the GMAT mission and vision statement. The GMAT mission statement is that it will study, develop, test, and transfer novel technologies and already existing space trajectories optimization and their mission design. The GMAT vision statement is to allow the creation of previously undeveloped space trajectory and mission design technologies. The motivation behind the GMAT was to reduce the large portion of the cost for the space communities. Also, to provide a test platform which NASA can use to develop, test and verify new technologies. One of the most important aspects that this paper shows is the GMAT orbit determination vision, System components and interactions overview. In GMAT OD, it was stated that in order to uniquely define an orbit determination problem, a user must frequently provide hundreds of pieces of information ranging from clock drift parameters, process noise characteristics, spacecraft physical properties, ground station properties, and atmospheric modeling parameters, to name just a few. The Orbit determination objects and accompanying data in GMAT are divided into five types. Measurement Participants are first, Sensors are second, Estimators are third, and Measurements and Dynamics are fourth and fifth. Other than orbit determination systems and components there is also GMAT high-fidelity modeling that the paper explains. There are four important high-fidelity modeling that the GMAT provides; (1) Non-spherical Gravity Fields and Earth Tides, (2) Atmospheric Density, (3) 6DOF Attitude Dynamics and (4) Solar Radiation Pressure (Solar Radiation Pressure).

3 Methodology

3.1 Implementing Phobos and Deimos into GMAT

Although the moons of Mars are not present inside GMAT by default, it is possible to add Deimos and Phobos into GMAT manually. All the instructions below are created by referring to the user guide given in the references [8]. In order to implement the Moons of Mars program, we must download the ephemeris file for Demios and Phobos, from the link also given below [9]. On the website, the file **mar085.bsp** needs to be downloaded. After the file is downloaded, open GMAT. Phobos and Deimos need to be entered as moons of Mars manually, in order to do that, right-click on Mars under the Resource tree, SolarSystem folder.

1. Click ”Add” then click ”Moon”
2. Type Phobos then click ”OK”
3. Open the properties of Phobos by double-clicking it under Mars.
4. Enter the following (actual) values of Phobos under *Properties* tab, as seen in Fig. 2

   Mu: 0.00070934 km^3/sec^2

   Equatorial Radius: 13.5 km

   Flattening: 0.3185185185185186

   The PCK Files part is left empty.

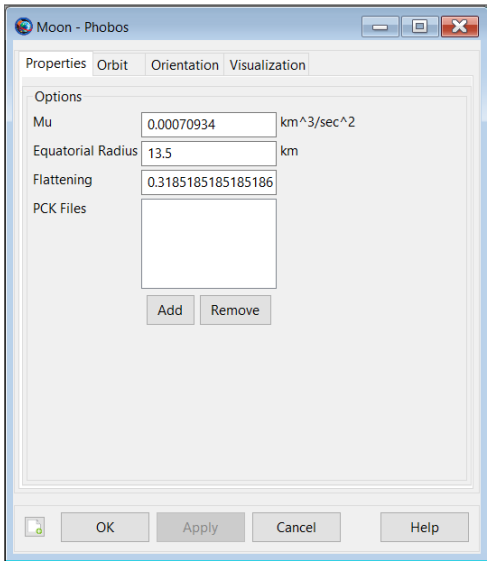

Figure 2: Entering the Orbit of Phobos

5. Under the *Orbit* tab, make sure the **Ephemeris Source** is SPICE (only available option) and in the **NAIF IF** box, enter 401 (international identification number for Phobos).

6. In the **SPK Files** click *Add* and select the path where the **mar085.bsp** file was downloaded (Fig. 3). Then click OK.

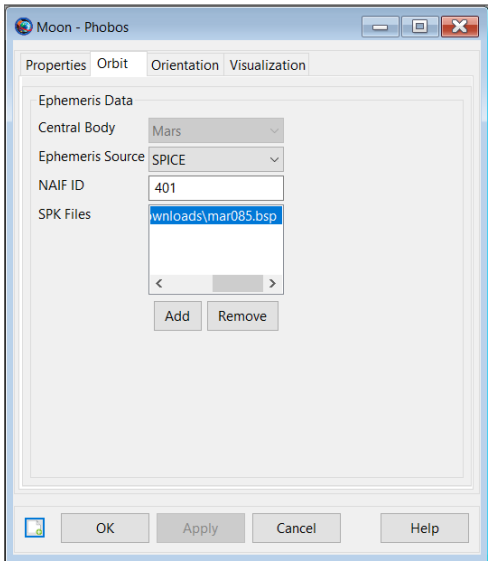

Figure 3: Entering the Orbit of Phobos

Phobos is successfully added as a moon of Mars. Next, repeat the same steps for Deimos, with the values below;

Name: Deimos
Mu: 0.000158817 km^3/sec^2
Equatorial Radius: 7.5 km
Flattening: 0.3066666666666666
The PCK Files part is left empty.

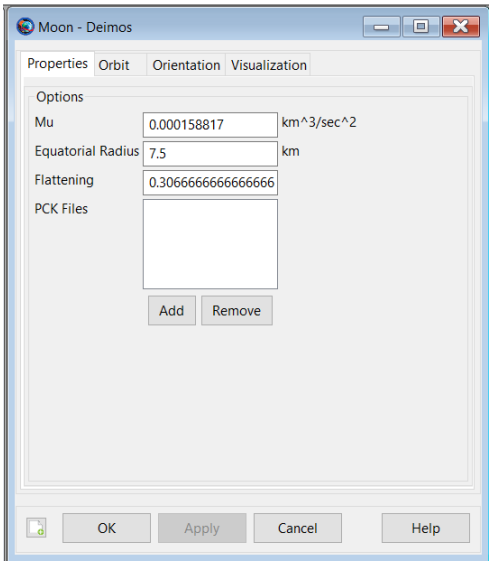

Figure 4: Entering the Properties of Deimos

In the **SPK Files** click *Add* and select the path where the **mar085.bsp** file was downloaded. Then click OK.

Under the *Orbit* tab;

NAIF ID: 402 (international identification number for Deimos)

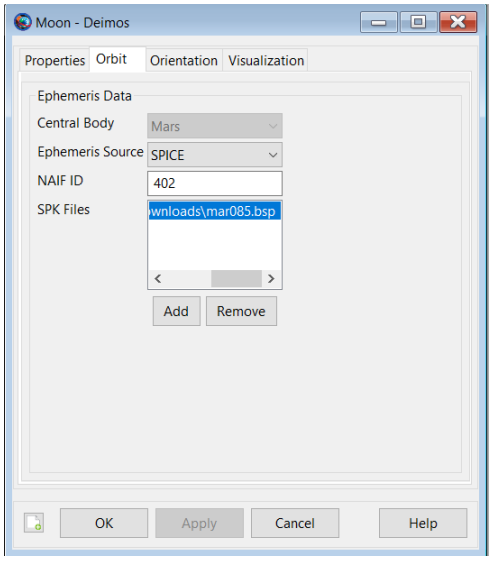

Figure 5: Entering the Orbit of Deimos

After implementing both moons of Mars, we can create a propagator including

Phobos and Deimos.

1. Under the **Resources** tree, right click on **Propagators** and click *Add Propagator*. Double-click on this propagator to edit its properties.
2. Under **Force Model**, select Mars as the *Central Body*
3. Similarly, select Mars as the *Primary Body*
4. Under **Gravity** select Mars-50c in the *Model* list.
5. In the **Degree** and **Order** boxes, type 4 and 4, respectively.
6. Select Deimos and Phobos (alongside the bodies of your choice) in the **Point Masses** part.
7. Check the *Use Solar Radiation Pressure* box.
8. Click *Apply*, then *OK*.

After the propagator has been added, go to the **Output** file under the **Resources** tree, and double-click on *OpenFrames1*. Under the **Celestial Object** part, select Phobos and Deimos and click on the right arrow to put them under **Selected Celestial Object**. Repeat this step for *OpenFrames2*. This will allow Deimos and Phobos to be visible in the simulation.
If everything is done correctly, Phobos and Deimos are added to the system.

3.2 Adding New Spacecraft into GMAT

One of the key goals of this mission was to observe and analyze the positions of spacecraft that are already in orbit around Mars. For this purpose, MEX, MAVEN and 2001 Mars Odyssey are added to the system manually. The analysis of their orbits and their positions at impact will be discussed in Sec. 4.2. This section will act as a guide to implementing new spacecraft into the script. This section will show the process for MAVEN only, unless stated otherwise.

The orbital elements of any major body or most spacecraft can be obtained from JPL's Horizons System. Below, the main interface of the web program is seen. In the Ephemeris Type, "Osculating Orbital Elements" must be selected in order to obtain the needed information. Below, the coordinate system can be selected by the user, for the case of this study, Mars (body center) is chosen. In the "Time Specification" section, the start and stop times are entered into the system. For some spacecraft, like MEX and Mars Odyssey, this range is very short, hence extrapolation is needed for this study, as will be discussed in later sections. The

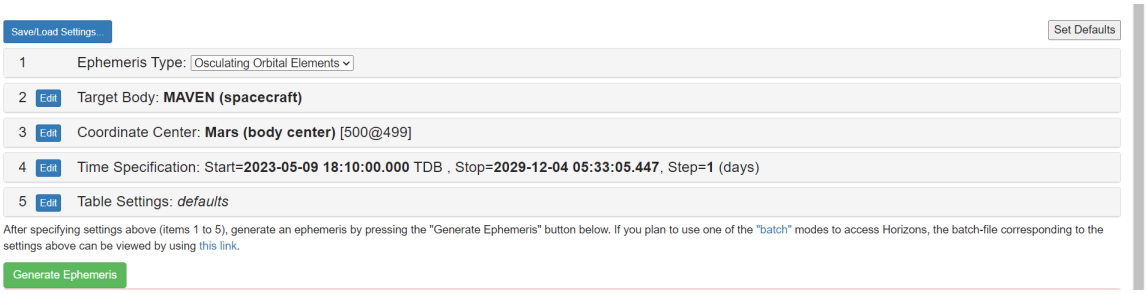

Figure 6: JPL Horizons System Main Interface

step size can also be altered from the same section, with the number of data points increasing as step size decreases.

After clicking on “Generate Ephemeris”, a text file can be downloaded from the system. A set of 12 elements are obtained, which are the orbital elements that will be entered into GMAT when creating the spacecraft. In the figures below, the elements of MAVEN at impact date are given. As the simulation of the orbiters starts one day prior to the impact date, the orbital elements on December 3rd are of importance.

In GMAT, right-clicking on Spacecraft and clicking on “Add Spacecraft”, a new entry will be added. In the new entry, Epoch is entered as a day before the impact date for all orbiters, along with selecting “Keplerian” as the state type, which allows the user to enter orbital elements. In the coordinate system, “MarsFixed” is selected since all of the added spacecraft will be in orbit around Mars. From there, the orbital elements are entered and the spacecraft is created. Other properties such as “DryMass” can be entered under the “Ballistic/Mass” tab.

After all the spacecraft have been added to the system, a propagator must be prepared to apply to the orbiters. Since the solar-sailed spacecraft is in orbit around the Sun and the orbiters are around Mars, the propagators must be different. Double-clicking on the propagator which is named “MarsSAT” in this study, opens the “PropSetup” window. On the left side of this window, minimum and maximum step sizes are significant and need to be changed according to the user. Since the period of revolution is under half a day, the minimum and maximum step sizes that are used in the main propagator, will not yield accurate results for the orbiters. Therefore, step sizes are significantly decreased to allow the user to see the changes in the orbits of the spacecraft. Since the step size and computational time are inversely proportional, the speed of the simulation decreases on the last day of the mission, where the orbits of MEX, MAVEN and Mars Odyssey are also included. On the right side of the window, “Central Body” and “Primary Body” are selected as Mars for this mission as seen in Fig. 14, since this propagator is for the orbiters. Below, all major bodies apart from Mars (which is the primary body)

```
 EC= 3.6647775538367 64E-01 QR= 3.587823794586585E+03 IN= 5.546092204121273E+01
 OM= 2.145824140856218E+02 W = 3.516594341676059E+02 Tp=  2462474.121345794760
 N = 2.782175796055753E-02 MA= 6.402260435231284E+01 TA= 1.067111887366642E+02
 A = 5.663295685472667E+03 AD= 7.738767576358749E+03 PR= 1.293951304264692E+04
2462474.231313044 = A.D. 2029-Dec-03 17:33:05.4470 TDB
 EC= 3.6672410939502 68E-01 QR= 3.592326172925155E+03 IN= 5.549237598465756E+01
 OM= 2.145524757497604E+02 W = 3.517982784542608E+02 Tp=  2462474.271439040545
 N = 2.775327324516379E-02 MA= 2.637825636188451E+02 TA= 2.267068222457684E+02
 A = 5.672608457418738E+03 AD= 7.752890741912321E+03 PR= 1.297144292926719E+04
2462474.314646377 = A.D. 2029-Dec-03 19:33:05.4470 TDB
 EC= 3.6716181218944 65E-01 QR= 3.586233433098787E+03 IN= 5.552568655047580E+01
 OM= 2.144329597136251E+02 W = 3.516522171257161E+02 Tp=  2462474.271451816894
 N = 2.779518753473778E-02 MA= 1.037319183108518E+02 TA= 1.383949705567809E+02
 A = 5.666904276915036E+03 AD= 7.747575120731286E+03 PR= 1.295188239151401E+04
2462474.397979711 = A.D. 2029-Dec-03 21:33:05.4470 TDB
 EC= 3.6687723548565 18E-01 QR= 3.587842799938084E+03 IN= 5.552516899975524E+01
 OM= 2.144061975157224E+02 W = 3.518478169592566E+02 Tp=  2462474.421496690251
 N = 2.779522590703984E-02 MA= 3.035237964750702E+02 TA= 2.611474827624938E+02
 A = 5.666899061338007E+03 AD= 7.745955322737931E+03 PR= 1.295186451097780E+04
2462474.481313044 = A.D. 2029-Dec-03 23:33:05.4470 TDB
 EC= 3.6700901520207 90E-01 QR= 3.589013690696969E+03 IN= 5.555705188155192E+01
 OM= 2.142731635044722E+02 W = 3.516335166006297E+02 Tp=  2462474.421512179542
 N = 2.777295166104887E-02 MA= 1.434971392346611E+02 TA= 1.614664152883682E+02
 A = 5.669928604585636E+03 AD= 7.750843518474303E+03 PR= 1.296225206429515E+04
2462474.564646377 = A.D. 2029-Dec-04 01:33:05.4470 TDB
 EC= 3.6442231515544 74E-01 QR= 3.592926839638575E+03 IN= 5.556549574390769E+01
 OM= 2.142085331203832E+02 W = 3.516656946501851E+02 Tp=  2462474.571581657976
 N = 2.789772723566163E-02 MA= 3.432834510992323E+02 TA= 3.228910660122588E+02
 A = 5.653009734785324E+03 AD= 7.713092629932074E+03 PR= 1.290427700288834E+04
2462474.647979711 = A.D. 2029-Dec-04 03:33:05.4470 TDB
 EC= 3.6661595498601 00E-01 QR= 3.592479044595123E+03 IN= 5.559762755193243E+01
 OM= 2.141204385883288E+02 W = 3.514926051486951E+02 Tp=  2462474.721663808450
 N = 2.775861141517554E-02 MA= 1.832801845094991E+02 TA= 1.816342942985760E+02
 A = 5.671881179949477E+03 AD= 7.751283315303831E+03 PR= 1.296894843245614E+04
2462474.731313044 = A.D. 2029-Dec-04 05:33:05.4470 TDB
 EC= 3.6675839491394 03E-01 QR= 3.595455936038976E+03 IN= 5.565647995911283E+01
 OM= 2.140514241455546E+02 W = 3.514941432183973E+02 Tp=  2462474.721646148246
 N = 2.771479236878374E-02 MA= 2.314794343623172E+01 TA= 5.008998957785225E+01
 A = 5.677858035797161E+03 AD= 7.760260135555347E+03 PR= 1.298945325693589E+04
$$EOE
******************************************************************************
```

Symbol meaning:

JDTDB	Julian Day Number, Barycentric Dynamical Time
EC	Eccentricity, e
QR	Periapsis distance, q (km)
IN	Inclination w.r.t X-Y plane, i (degrees)
OM	Longitude of Ascending Node, OMEGA, (degrees)
W	Argument of Perifocus, w (degrees)
Tp	Time of periapsis (Julian Day Number)
N	Mean motion, n (degrees/sec)
MA	Mean anomaly, M (degrees)
TA	True anomaly, nu (degrees)
A	Semi-major axis, a (km)
AD	Apoapsis distance (km)
PR	Sidereal orbit period (sec)

Figure 7: Orbital Elements Obtained from the Horizons System

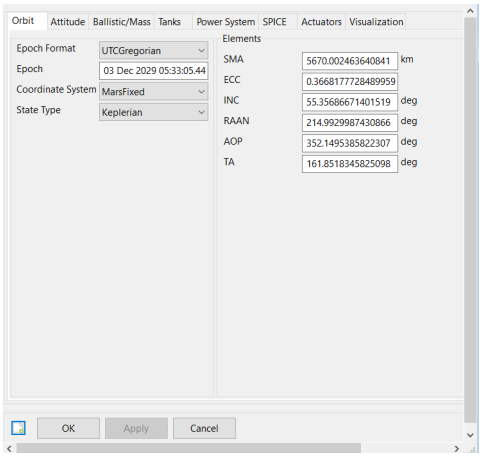

Figure 8: MAVEN Spacecraft Properties in GMAT

are entered as“Point Masses”. In correlation with the main mission of this study, Solar Radiation Pressure is also enabled, although it has a negligible effect on the spacecraft around Mars for this mission.

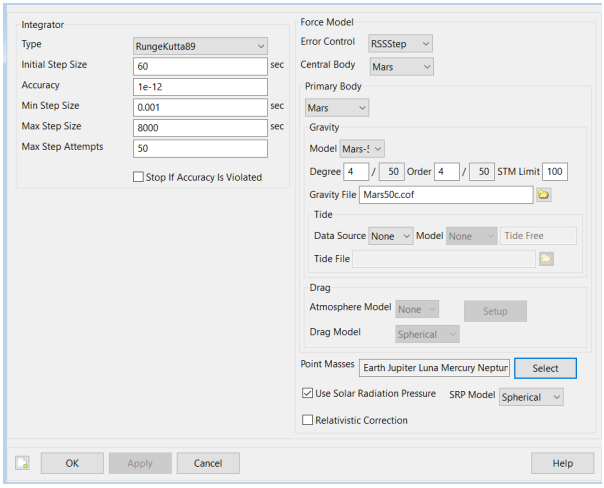

Figure 9: MarsSAT Propagator

Once the propagator is created, the mission sequence can be written. As can be followed in Fig. 10, the mission of this study begins with the solar-sailed spacecraft propagating towards its first periapsis. Once there, a continuous trajectory from apoapsis to periapsis is created with the use of a For loop. This loop continues for 6 iterations, where orbital energy increases with each iteration, which can of course be changed according to the mission. After the spacecraft reaches the SOI of Mars, where the radius of the SOI is taken as 578000 kilometers from Mars, created orbiters are simulated with the propagator. This step continues for a day, allowing the spacecraft to complete its orbits multiple times. After MEX, MAVEN and Mars Odyssey are simulated, the mission ends with an impact on Mars.

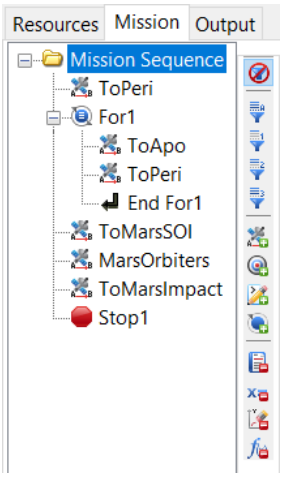

Figure 10: Mission Sequence

To observe the simulation and orbits of the three spacecraft added into the system along with Phobos and Deimos, an "OpenFramesInterface" output file must be added. In this file, any spacecraft and major body in the system can be selected to be visible during the simulation. An important part of the mission was to include a flyby to one of the Martian moons and the aim was to direct the onboard camera toward the moon to enable a detailed analysis of its surface and possible atmosphere. This flyby will be discussed in more detail in Sec. 4.4.2. The hypothetical camera is created as can be seen in Figs. 11 and 12, where the "Maintain view direction toward object" box must be checked and the required body must be selected. As will be seen in later Sections, this allows the observer to watch the simulation while the center of the FOV is set as the given body.

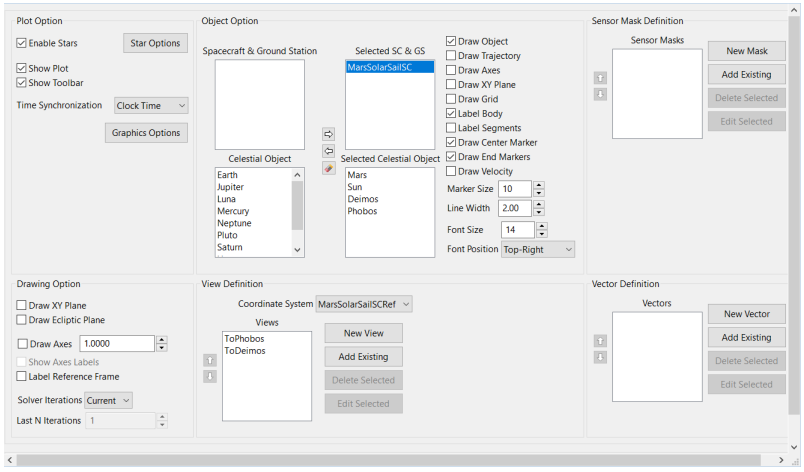

Figure 11: Creating OpenFrames for the Orbiters

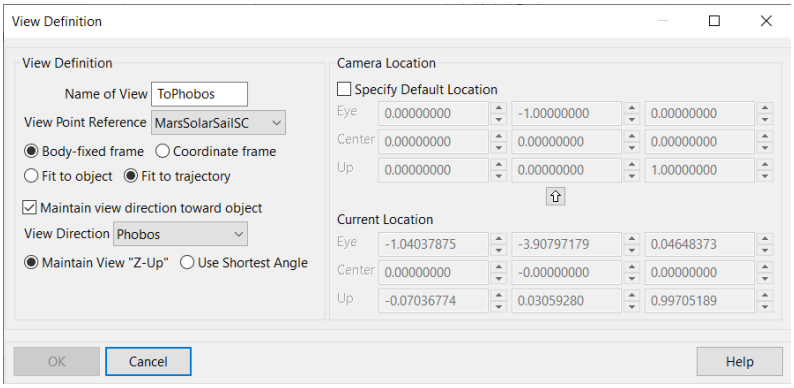

Figure 12: Adjusting the Camera to Observe the Moons

3.3 The Force on a Sphere in GMAT

In order to prove the force acting on a sphere (by solar radiation pressure for our study), the effects of Solar Flux (denoted with SRP.Flux in the script) and the coefficient of reflectivity are compared.

The default value of SRP Flux in GMAT is 1367, and the coefficient of reflectivity (η) of the sails of our spacecraft is experimentally chosen as 0.8. Firstly, SRP Flux is decreased to 90% of its default value, which is equal to 1230.3. Without changing the coefficient of reflectivity, the Sun Eccliptic velocity is noted along the 6th orbit.

Repeating the same process for the coefficient of reflectivity, the value was decreased from 0.8 to 0.72, while keeping the SRP Flux constant at default. It is seen that all the values are identical throughout the orbit, where the velocity ranges from 14.60908190128852 to 67.66407190601404 kilometers per second. This experiment has proved that the force on a sphere is indeed;

$$F = \eta \frac{I \pi R^2}{c} \tag{10}$$

where η is the coefficient of reflectivity, I is the SRP Flux, R is the radius of the sphere and c is the speed of light.

3.4 Heliocentric solar-sailing - Mathematica

It is important to compare the obtained results with the analytical approach. For this case, the analytical rise of the aphelion is derived as seen below. The following work is done with reference to [10].

$$I(r) = \sigma_{SB} T_{\odot}^4 \frac{{R_{\odot}}^2}{r^2} = \frac{L_{\odot}}{4\pi r^2}\,. \tag{11}$$

where

$$L_\odot = 4\pi\sigma_{SB}T_\odot^4 {R_\odot}^2 \tag{12}$$

$$k_{eff} = k_\odot - \frac{\pi R^2}{m_{SC}}\frac{L_\odot}{4\pi c}, \tag{13}$$

By calculating the effective gravitational parameter on the outbound arc, we can then calculate the angular momentum, by means of SMA and ECC.

$$\ell_{a,p} = r_{a,p}v_{a,p} = \sqrt{k_{eff}a(1-e^2)} \tag{14}$$

Continuing, the SMA and ECC in the "On" position can be obtained as below. These equations allow having an analytical approach to the rise of the apoapsis.

$$a = \frac{k_{eff}r_p}{2k_{eff} - r_p v^2} \tag{15}$$

$$e = \frac{-k_{eff} + r_p v^2}{k_{eff}} \tag{16}$$

From the equations obtained below, a plot comparing the analytical rise of the aphelia to the GMAT solution is derived. It can be seen in Fig. 13 that the rise of aphelion does converge to the analytical solution.

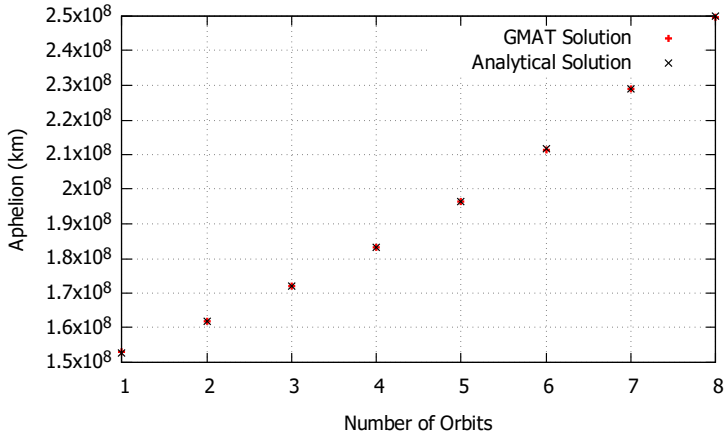

Figure 13: Analytical Rise of the Aphelia

4 Results and Discussion

4.1 Dependence on Coefficient of Reflectivity

To create a realistic mission, the coefficient of reflectivity (η) has been decreased from 1.8 to 0.8. The coefficient of reflectivity has a range of $0 \leq \eta \leq 2$, where 0 means that no momentum is transferred from photons to the sail, 1 means all of the photons are absorbed and a maximum value of 2 means that all of the photons are reflected from the sail, therefore a maximum amount of momentum is transferred. The solar-sail powered spacecraft in this mission uses a reflector with $\eta = 0.8$. To understand the importance of the coefficient, Fig. 14 is derived. The dependency of spacecraft velocity versus the distance from the Sun to the coefficient is analyzed with 8 different values of η.

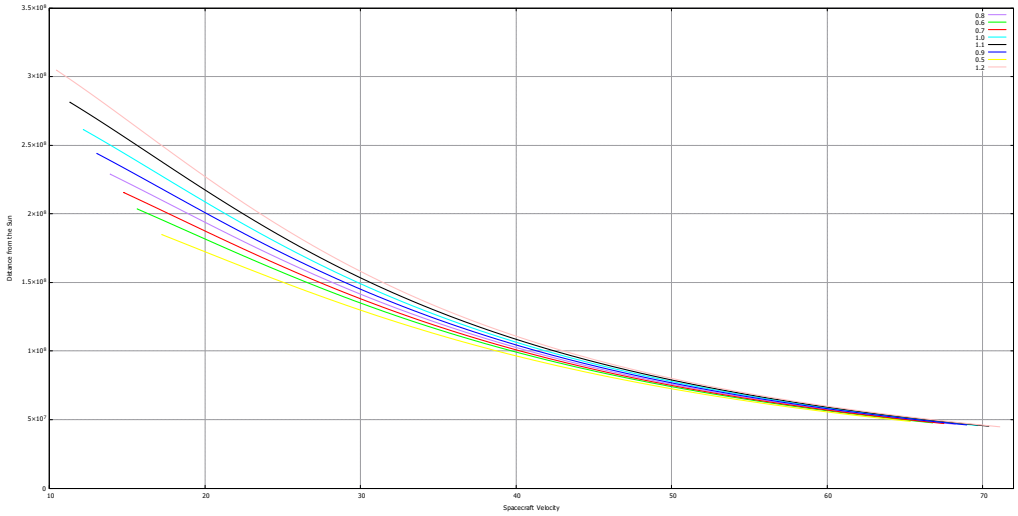

Figure 14: Instantaneous velocity versus Distance from the Sun

From this graph, the direct correlation between η and v can be observed. For each test, the 6th orbit of the spacecraft around the Sun is plotted, and therefore the range of v and distance is shown. It is clear that the differences in velocities are caused by the increased eccentricity as η increases. Gained orbital energy is directly proportional to η, therefore the aphelion is reached later in the orbit as the coefficient is increased. In accordance with Kepler's Second Law, velocity is inversely proportional to the distance from the Sun, which is also proven by looking at how different the velocities on the aphelion and on the perihelion change.

4.2 Implementing Orbiters into GMAT

In order to create a realistic mission, other orbiters around the red planet must also be discussed. Implementing other orbiters into the mission script of this study also creates more context and reference to the main solar-sailed spacecraft. There have been plenty of spacecraft both orbit and land on Mars throughout space exploration history. Although no mission with a solar-sail powered spacecraft has successfully completed an interplanetary mission, the orbits of the spacecraft that will be discussed below create a frame of reference for this mission.

Implementing the spacecraft into the main mission script was possible using Jet Propulsion Laboratory's Horizons System, which enables the user to generate osculating orbital elements for all the spacecraft on the database given a specific time and reference frame. For this purpose, NASA's Mars Atmosphere and Volatile Evolution (MAVEN), NASA's Mars Odyssey and ESA's Mars Express (MEX) are analyzed. Although the "Start" and "Stop" times for MAVEN are within the mission duration of this study, this is not the case for the latter two spacecraft, which will be discussed in more detail in Sec. 4.2.2 and Sec. 4.2.3. The extrapolated orbital elements are as found in Tab. 1.

Table 1: Extrapolated Orbital Elements of the Orbiters on 03 Dec 2029

	MAVEN	**MEX**	**Mars Odyssey**
SMA (km)	5670.002463643596	8820.596520171119	3794.468781896034
ECC	0.3668177728483931	0.5671549300004276	0.00953295900314563
INC (deg)	55.3568667140117	101.5733963999833	74.83774652293468
RAAN (deg)	214.9929987430832	14.9606474599781	311.218763788053
AOP (deg)	352.1495385820855	126.2967970000086	248.4768618090614
TA (deg)	161.8518345825982	181.0598439999994	100.9383727210037

Since the duration of the mission is approximately 6.5 years, it is difficult to simulate the orbits of the three spacecraft for the entirety of the mission, given that their periods of revolution are less than half a day. For this purpose, the Epoch of all the orbiters is chosen (03 Dec 2029 05:33:05.447) exactly one day before the impact date. As will be discussed in later sections, the orbital elements of the spacecraft at this date are either extrapolated (MEX and Mars Odyssey) or taken directly from the Horizons System (MAVEN). This allows the mission to simulate the orbits of all the spacecraft in the mission; MAVEN, MEX, Mars Odyssey and the main solar-sailed spacecraft, with less computational time and more accuracy. In order to visualize the three spacecraft, their orbits are given below in Figures 15a to 18d for a period of 30 days.

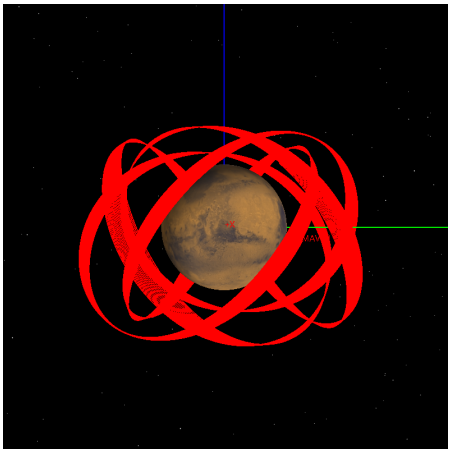

(a) MAVEN Orbit

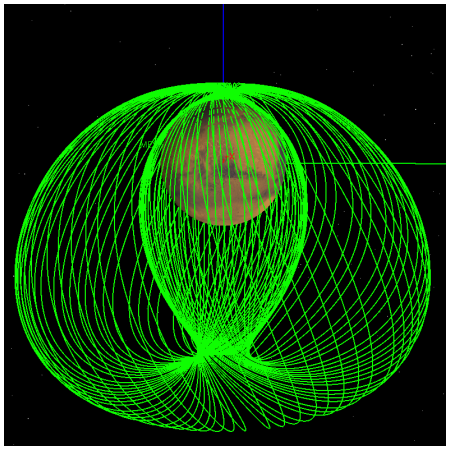

(b) MEX Orbit

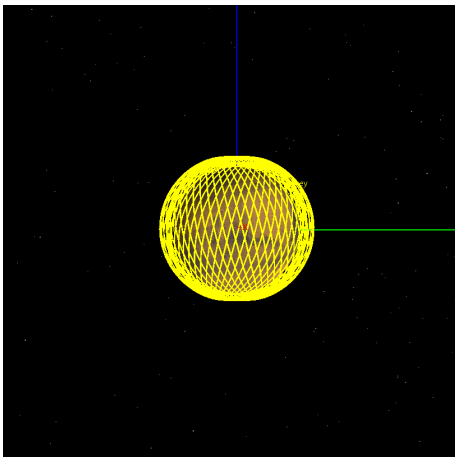

(c) Mars Odyssey Orbit

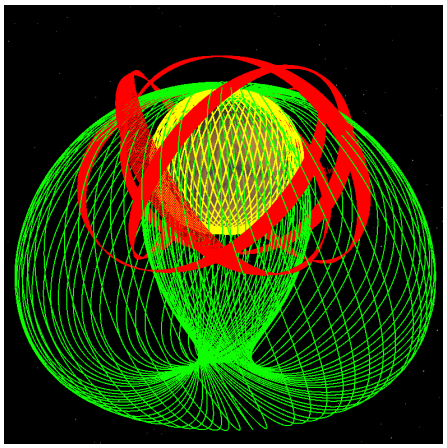

(d) Complete Orbit

Figure 15: Orbits of the 3 spacecraft for a period of 30 days

The differences in orbits can be observed above. The three spacecraft have very different eccentricities, resulting in very different orbits. The orbit of Mars Odyssey takes the least time to complete an orbit with a highly circular orbit, while Mars Express, with a quite elliptical orbit, takes the most time to go around Mars. Since the positioning of the orbiters is highly significant to avoid a collision with the incoming spacecraft, analysis of the orbits has very significant importance. The positioning and distances at the time of impact will be discussed in more detail in Sec. 4.3.

4.2.1 MAVEN

Mars Atmosphere and Volatile Evolution is the last mission to be successfully operated under NASA's Mars Scout Program [11]. The main objective of the mission is to analyze whether the loss of atmospheric gas in the Martian atmosphere to space, had significant effects on the change of climate of Mars [12]. For a better understanding of the atmosphere, the spacecraft was designed to aerobrake and execute 5 "deep-dip" campaigns, where the periapsis of the orbit decreases from 150 to 125 kilometers [13].

NASA's Mars Atmosphere and Volatile Evolution (MAVEN) is added to the script first. The orbital elements are gathered from JPL's Horizons System. Since the "start" and "stop" dates in Horizons for MAVEN are inside the mission duration, no extrapolation is used. The osculating orbital elements of MAVEN on the date **2029-12-03 05:33:05.446** are as seen in Tab. 1.

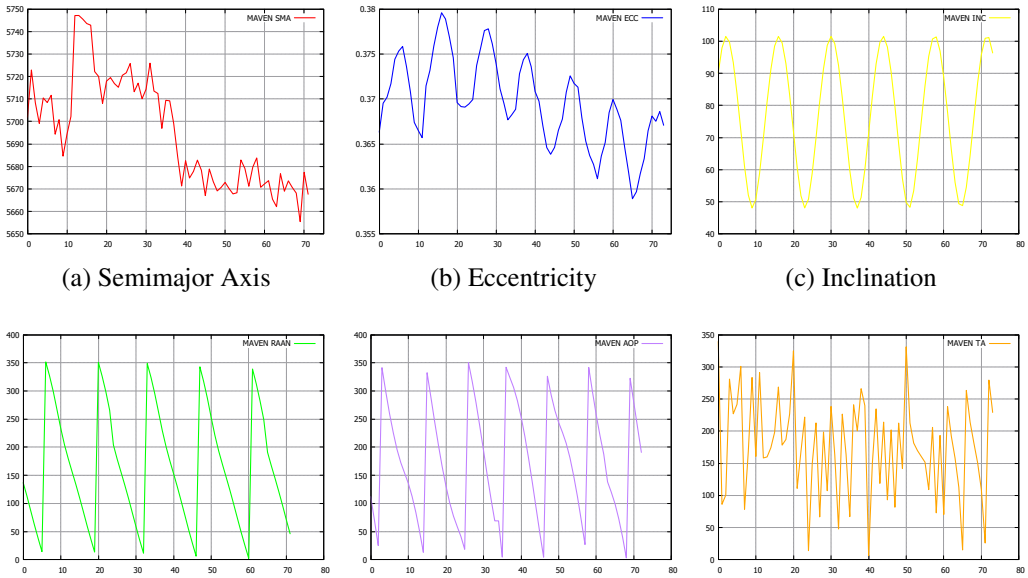

(a) Semimajor Axis (b) Eccentricity (c) Inclination

(d) RAAN (e) Argument of the Periapsis (f) True Anomaly

Figure 16: Change in the Orbital Elements of MAVEN

4.2.2 Mars Express

Mars Express (MEX) is the first European interplanetary mission, launched in 2003. Along with the great coverage of Mars that MEX have provided, the mission also aims to look for traces of past biological life, through ice and water [14]. As will be discussed in the next paragraph, it has a highly elliptical orbit compared to other orbiters, with a periapsis of about 270 kilometers and a period

of revolution of 6.75 hours [14]. MEX is also an important part of this study since Solar Radiation Pressure was given high importance for orbit determination. For this purpose, a physical model of the spacecraft was designed by JPL, where a 6-component model was implemented [15].

As discussed in Sec. 4.2, the orbital elements of MAVEN, Mars Express and Mars Odyssey are taken from NASA's Horizons System. In Horizons, the latest "Stop time" for Mars Express is **2029-01-01 12:01:09.184**, which is before the impact date of our spacecraft, on **2029-12-04 05:33:05.446**. For this case, the osculating orbital elements of Mars Express (MEX) are gathered from the launch date (09 May 2023 18:10:00.000) to the latest stop time, with a step size of 30 days. Each orbital element is plotted and then the values at the impact date are estimated with extrapolation. The estimated values of Mars Odyssey are given in Tab 1. The change in the orbital elements of Mars Odyssey can be observed in Figures 17a to 17f.

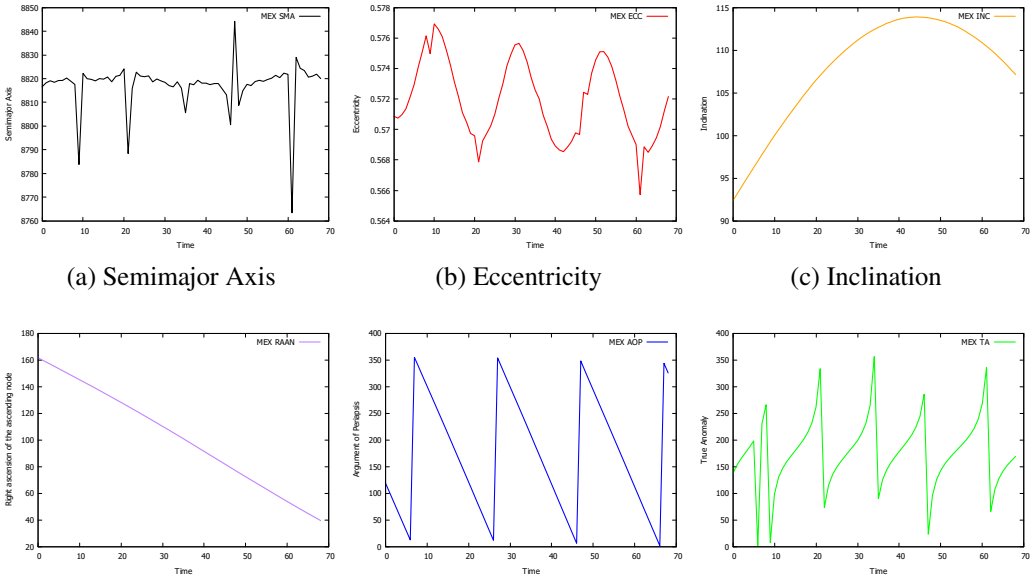

(a) Semimajor Axis (b) Eccentricity (c) Inclination

(d) RAAN (e) Argument of the Periapsis (f) True Anomaly

Figure 17: Change in the Orbital Elements of Mars Express

4.2.3 Mars Odyssey

2001 Mars Odyssey, launched on April 7, 2001, aimed to study the elemental composition of the surface of the red planet. Additionally, the mission was of high importance as it was planned to analyze the environmental radiation of Mars, providing crucial insight into whether it would be possible for humans to live

there in the future [16]. The mission also made use of aerobrake, decreasing the initial ECC in each orbit to have a more circular orbit. The orbital energy of the spacecraft is decreased during each periapsis, which is mentioned as a "drag pass" [17].

As discussed in Sec. 4.2, the orbital elements of MAVEN, Mars Express and Mars Odyssey are taken from NASA's Horizons System. In Horizons, the latest "Stop time" for Mars Odyssey is **2029-08-05 00:00:00.000**, which is before the impact date of our spacecraft, on **2029-12-04 05:33:05.446**. For this case, the osculating orbital elements of Mars Odyssey are gathered from 5 years prior (31 Aug 2023 00:00:00.000) to the latest stop time, with a step size of 30 days. Each orbital element is plotted and then the values at the impact date are estimated with extrapolation. The estimated values of Mars Odyssey are given in Tab. 1. The change in the orbital elements of Mars Odyssey can be observed in Figures 18a to 18f.

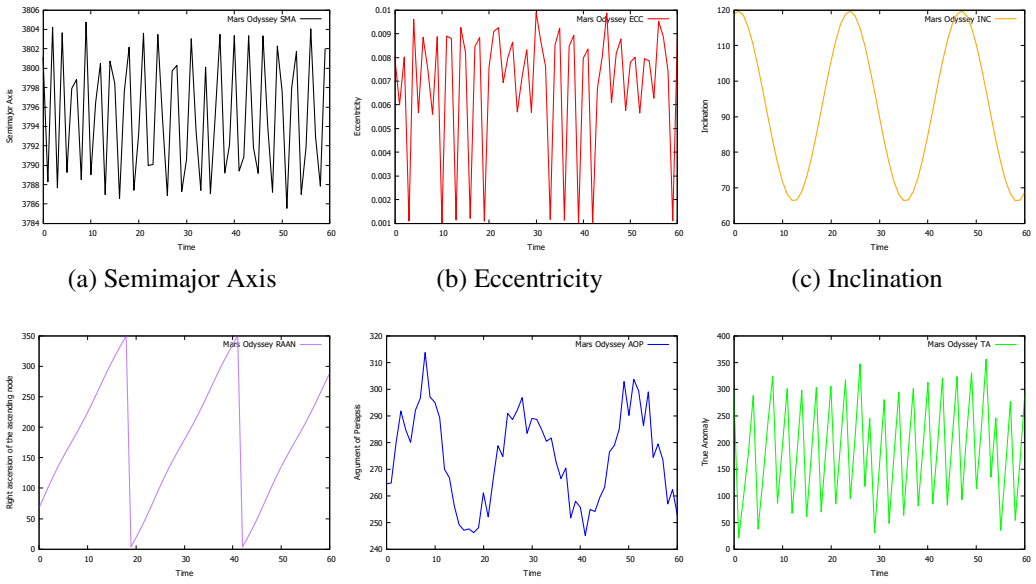

(a) Semimajor Axis (b) Eccentricity (c) Inclination

(d) RAAN (e) Argument of the Periapsis (f) True Anomaly

Figure 18: Change in the Orbital Elements of Mars Odyssey

4.3 Crash Avoidance

Crash avoidance is a crucial aspect of interplanetary missions, especially with Mars with a high number of orbiters. Without any engine on board, the solar-sail can not produce a Δv burn, therefore would not be able to effectively adjust its position according to the orbiters. For this case, the distances between the orbiters

are simulated upfront to be aware of the positions of the orbiters. The simulation shows where the orbiters are at the time of impact, which is given below in Figs. 19a and 19b.

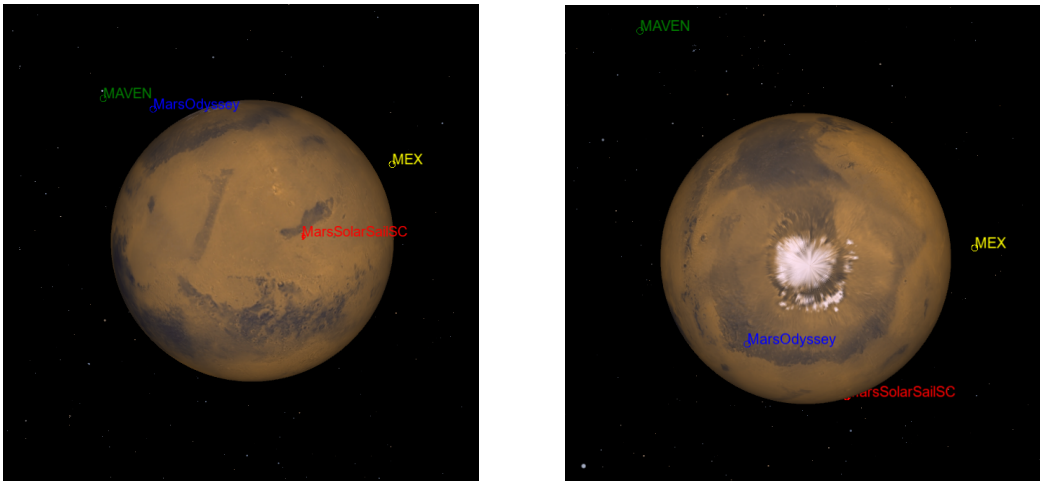

(a) (b)

Figure 19: Positions of the Orbiters at Impact

The distances between the spacecraft and the orbiters are plotted in Gnuplot and are given in Fig. 20. As can be observed, there is a sharp decrease in the distance as the spacecraft is approaching Mars and therefore the orbiters. In correlation with the figures above, Mars Odyssey is the closest orbiter to the spacecraft, and MAVEN, traveling towards its apoapsis, is the farthest. To calculate the Euclidean distance between two spacecraft, their MarsFixed X, Y and Z coordinates are noted and calculated as below [18]

$$SC1 = aX, bY, cZ$$

$$SC2 = iX, jY, kZ$$

$$|SC1 - SC2| = \sqrt{(a-i)^2 + (b-j)^2 + (c-k)^2} \tag{17}$$

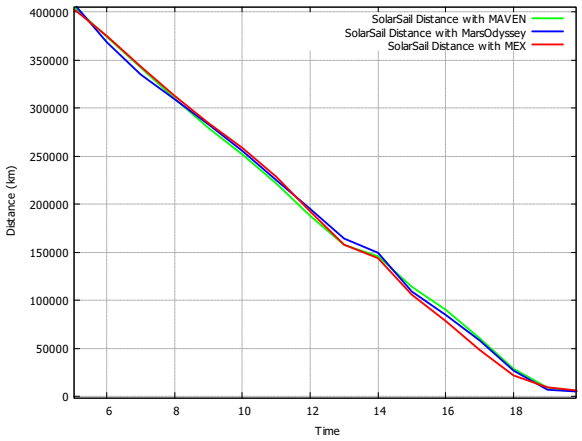

Figure 20: Distance between the Spacecraft and Orbiters

Table 2: Distance between the Orbiters During the Last 3 Hours

	MAVEN	**MEX**	**MarsOdyssey**
04 Dec 2029 02:36:04.712	157575.78	157823.18	164233.04
04 Dec 2029 02:50:04.283	145796.99	143808.71	149462.71
04 Dec 2029 03:28:22.302	114060.85	105794.32	109158.49
04 Dec 2029 03:56:31.499	90070.220	78352.341	84753.819
04 Dec 2029 04:28:17.439	60521.321	48424.752	58308.152
04 Dec 2029 04:59:13.255	28769.653	21932.913	7084.31539
04 Dec 2029 05:18:01.254	9260.6514	9564.2169	26935.5512
04 Dec 2029 05:26:08.599	4839.9007	5927.2659	4890.45977

4.4 Phobos and Deimos

4.4.1 Martian Moons Orbits

After the Martian moons are implemented into GMAT, as discussed in Sec. 3.1, their positions throughout the mission are gathered and plotted to get a better understanding of their orbits. To get meaningful results and plot their orbits, MarsFixed reference frame is selected and the moons' X, Y and Z coordinates are entered into Jupyter Notebook and plotted with the Mathematica kernel. In Figs. 21a and 21b, the orbits of Phobos and Deimos are seen respectively. Although they appear similar, in Fig. 21c, we observe how much wider and more massive Deimos' orbit is compared to Phobos'.

Both moons have very low ECC values, resulting in circular orbits. Deimos has the lower eccentricity, with 0.0003 compared to Phobos' 0.015. Similarly,

Deimos has a lower inclination than Phobos, 0.93° and 1.093° respectively [19]. Although the differences may seem small enough to be disregarded, the 50 times more eccentric orbit of Phobos along with a higher inclination, results in the orbit seeming smaller than it already is in Fig. 21c.

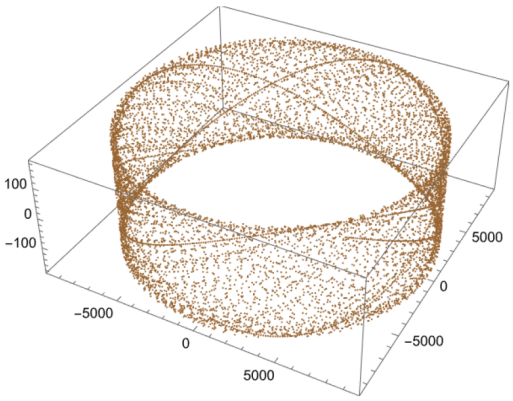

(a) Phobos Orbit

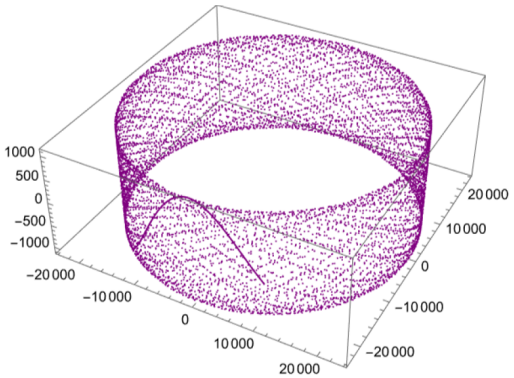

(b) Deimos Orbit

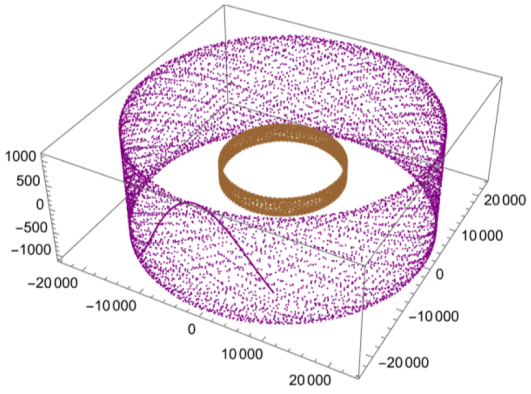

(c) Both Orbits

Figure 21: Martian Moon Orbits Plotted with Mathematica

The points seem orderly distributed, apart from the thread at the end of the orbit of Deimos. When the mission sequence advances to "MarsOrbiters" from "ToMarsSOI" as seen in Sec. 3.2, step size decreases significantly since the program begins to simulate the orbits of MAVEN MEX and Mars Odyssey. Meanwhile, Phobos and Deimos continue their orbits around Mars, although much slower with the decreased step size. More data points are generated by decreasing the step size, therefore we observe a more continuous thread, which is also more accurate.

4.4.2 Martian Moons Flyby

Another important goal of this mission was to enable Martian moon flybys. The moons of the red planet are not deeply observed and studied, partly because of their non-spherical shapes and they are very small compared to other moons of the solar system. To design a trajectory that allowed flybys, Phobos and Deimos are added to GMAT manually, as discussed in Sec. 3.1. The moons are similarly added also to AstroGrav, to find the arrival date which allowed a double flyby. Due to their fast velocities, a double flyby, where the spacecraft would have been able to observe both Phobos and Deimos, had a very short possible window. Since this was not possible alongside the main mission, flybys to both moons are done separately. The orbital elements for the flybys for Phobos and Deimos can be observed in Tab. 3 below.

Table 3: Orbital Elements for Flybys

	Phobos Flyby	**Deimos Flyby**
SMA (km)	101920000.0000012	101919000.0000017
ECC	0.4999999999999942	0.4999999999999806
INC (deg)	2.044410000000016	2.041180000000284
RAAN (deg)	25.45999999999993	25.44009000000014
AOP (deg)	89.99500000000043	89.9950010000219
TA (deg)	99.98915000000000	99.98915000000342
Distance (km)	55.75386470022779	106.7188439602449

The closest approaches to each moon can be observed in Figs. 22a and 22b below. For the flyby of Phobos, the spacecraft approaches the moon behind Mars, hence we see the dark side of the red planet. In comparison, both Deimos and Mars are much clearer in the second flyby, as the spacecraft records the minimum distance to the moon while on the day side of Mars. The orbits and radii of the moons also can be observed as Phobos appears much more massive than Deimos. For both of these flybys, the camera onboard the spacecraft is directed to the moons, allowing the mission to examine and analyze the moons of the red planet in more detail.

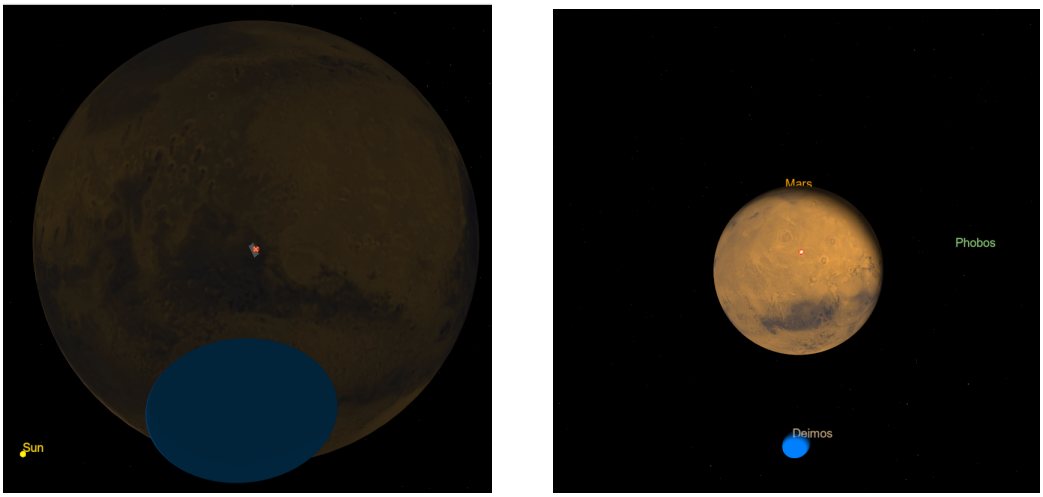

(a) Phobos (b) Deimos

Figure 22: Closest Flybys to (a) Phobos and (b) Deimos

Although the values above yield the closest approaches to the moons, the mission fails to have an impact on Mars. Therefore, the aim was to create a mission that had success in both a flyby and reaching Mars. The elements below in Tab. 4 are found and tested to be ideal for including a flyby into the main mission. By comparing the two tables, it is clear how sensitive the orbital elements are to change, with a slight change resulting in a difference in thousands of kilometers.

Table 4: Orbital Elements for Phobos Flyby with Mars Impact

	Phobos Flyby 2
SMA (km)	101920000.0000012
ECC	0.4999999999999942
INC (deg)	2.043905000000000
RAAN (deg)	25.46200000000008
AOP (deg)	89.995150000000009
TA (deg)	99.98919999999993
Distance (km)	5323.782113136071

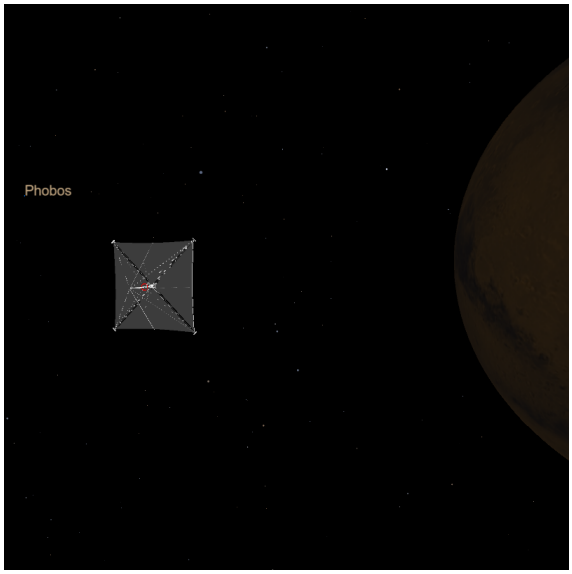

Figure 23: Phobos Flyby in the Main Mission

4.5 SPAD File Implementation

For this study, a cannonball model SPAD is created and implemented into the program by referring to the work of Pinto (2023) [20]. In order to compare the orbits with and without SPAD files, a simple MEO is defined as seen in Fig. 24. The eccentricity of this orbit is defined as 0 to further observe the differences in both ECC and SMA. Firstly in Fig. 25, altitudes are compared in 2 cases: 1) non-SPAD, GMAT Spherical Method, and 2) Cannonball approximation. The initial parameters are set as the actual mass, area and reflectivity values of the main spacecraft. The spacecraft is put in an orbit with a semi-major axis of 17095 km. It is observed that by decreasing the SRP Area in GMAT from 900 m^2 to 200 m^2, the altitudes match for the first 10 orbits of the spacecraft. As expected, maximum altitude increases for both cases in each orbit, using only Solar Radiation Pressure. It is worth noting that, as stated in previous sections, higher-fidelity models would have generated more accurate results, in exchange for more computational time.

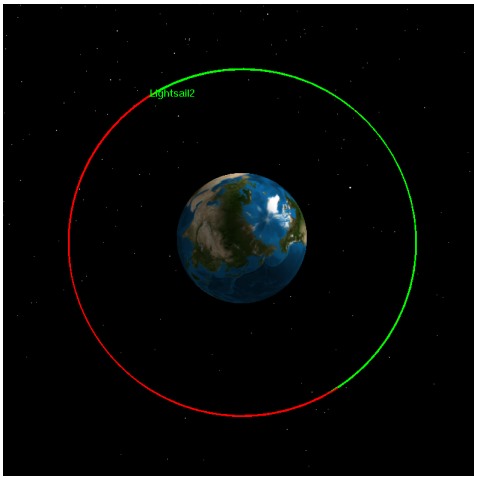

Figure 24: 0 eccentricity orbit

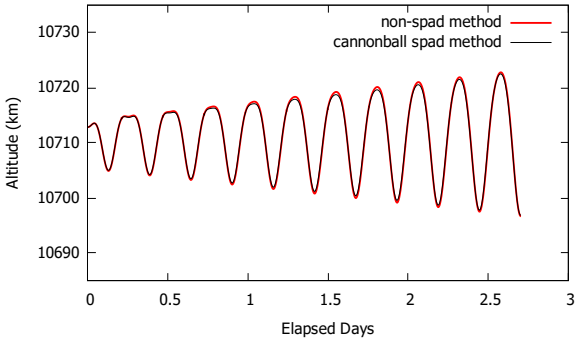

Figure 25: Difference in Altitude for Spherical and Cannonball Methods

Next, without changing any of the initial parameters of the initial spacecraft, the differences in the cannonball model SPAD and GMAT's automatic Spherical model is analyzed. With this approach, the significance of solely the SPAD files is aimed to be observed. To get a better understanding, the number of orbits is increased from 10 to 20. In Fig. 26a, the change in eccentricity with the Spherical model is seen to be increasing much more rapidly than the case with the cannonball model. Along with the eccentricity, the change in the semi-major axis is also analyzed, as seen in Fig. 26b. In correlation with the results obtained by T. Williams and colleagues [5], the Spherical Solar Radiation Pressure method used by the program provides a more significant increase in the gained orbital energy in each orbit. Contrarily, the cannonball model yields more realistic results, therefore the change in the orbit is less effective in terms of eccentricity and semi-major axis.

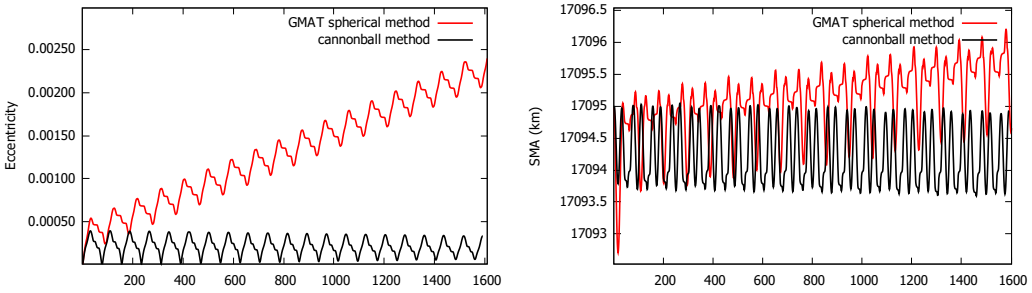

(a) eccentricity

(b) semi-major axis

Figure 26: Differences in SMA and ECC with/without SPAD

5 Conclusions

In conclusion, different objectives have been completed. Firstly, the Martian moons Phobos and Deimos have been added to the script, making this project one of the very few to include the moons in GMAT. This objective was crucial to analyze and see the trajectorial behavior of the solar-sail propelled spacecraft. Continuing, the visualization of the Martian moons of Phobos and Deimos and the flyby trajectory has been simulated through the program. Secondly, 3 currently operating orbiters around Mars; MAVEN, Mars Express (MEX) and Mars Odyssey have been implemented into the program, allowing the mission to have a crash avoidance segment. The purpose of this implementation is to help make the mission more realistic when designing the trajectory and flight dynamics of the spacecraft. Also, the graphs of the orbiters' distance over time and change in time over the orbital parameters of SMA, ECC, TA, AOP, INC and RAAN has been plotted. From the data obtained via Horizons System, the orbital elements are extrapolated according to the mission duration. The extrapolated elements were used to determine the position of each spacecraft during impact, which is crucial for crash avoidance studies. The importance of crash avoidance was to demonstrate that the spacecraft might be interrupted by another spacecraft or a celestial body like the Martian moons, which would have a high effect on the orbit of the spacecraft. It was understood that in the event of possible collision with another spacecraft, a small alteration of the sails of the spacecraft would be performed to prevent an accident. In addition, the importance of the change in the Coefficient of Reflectivity with respect to the Instantaneous velocity versus Distance from the Sun has been plotted and shown in this study. It was proven through GMAT that when the coefficient of reflectivity is increased, the maximum instantaneous velocity also increases. Lastly, a cannonball approximation is introduced to the

script for SPAD, also resulting in a more accurate approach. The use of an SPAD file for an interplanetary mission is difficult to operate, therefore this project aims to be a beginners guide in solar sailing.

In the future, more orbiters around Mars and in the Solar System can be added to GMAT to increase accuracy and make the mission more realistic. Also in addition to the orbiters, small asteroids, and orbital debris can be added into GMAT to significantly improve the mission quality.

References

[1] J. Grossman, Solar Sailing: The Next Space Craze?, Engineering & Science 63 (4) (2000) 18–29.

[2] J. R. Mansell, D. A. Spencer, B. A. Plante, M. A. Fernandez, C. T. Gillespie, J. M. Bellardo, A. Diaz, B. Betts, B. Nye, Orbit and Attitude Performance of the LightSail 2 Solar Sail Spacecraft (2019) 1–18.

[3] S. Boyd, The Dirac Equation (2015).

[4] L. Zardaín, A. Farrés, A. Puig, High-Fidelity Modeling and Visualizing of Solar Radiation Pressure: a Framework for High-Fidelity Analysis, Advances in the Astronautical Sciences 175 (2019) 3363–3382.

[5] T. W. Williams, K. M. Hughes, A. K. Mashiku, J. M. Longuski, Orbit Stability of Osiris-Rex in the Vicinity of Bennu Using a High-Fidelity Solar Radiation Model, Advances in the Astronautical Sciences 156 (2016).

[6] T. R. Lockett, L. Johnson, J. Matus, J. Lightholder, A. Marinan, A. Few, J. Castillo-Rogez, Near-Earth Asteroid Scout Flight Mission (10) (2019).

[7] L. G. Jacchia, Solar Effects on the Acceleration of Artificial Satellites (1963).

[8] GMAT Development Team, GMAT User Guide R2022a (2016).

[9] B. Semenov, R. Baalke, Jet Propulsion Laboratory - Planetary Data System (2023).
URL https://naif.jpl.nasa.gov/pub/naif/generic{_}kernels/spk/satellites/a{_}old{_}versions/

[10] F. Pinto, Heliocentric solar sailing . Note 1 (Jupyter Notebook v. 1.0) (2023).
URL https://osf.io/tehp2/

[11] P. K. Martin, Mars Atmosphere and Volatile Evolution (MAVEN) Project (2013).

[12] B. M. Jakosky, R. P. Lin, J. M. Grebowsky, J. G. Luhmann, D. F. Mitchell, G. Beutelschies, T. Priser, M. Acuna, L. Andersson, D. Baird, D. Baker, R. Bartlett, M. Benna, S. Bougher, D. Brain, D. Carson, S. Cauffman, P. Chamberlin, J. Y. Chaufray, O. Cheatom, J. Clarke, J. Connerney, T. Cravens, D. Curtis, G. Delory, S. Demcak, A. Dewolfe, F. Eparvier, R. Ergun, A. Eriksson, J. Espley, X. Fang, D. Folta, J. Fox, C. Gomez-Rosa, S. Habenicht, J. Halekas, G. Holsclaw, M. Houghton, R. Howard, M. Jarosz, N. Jedrich, M. Johnson, W. Kasprzak, M. Kelley, T. King, M. Lankton, D. Larson, F. Leblanc, F. Lefevre, R. Lillis, P. Mahaffy, C. Mazelle, W. McClintock, J. McFadden, D. L. Mitchell, F. Montmessin, J. Morrissey, W. Peterson, W. Possel, J. A. Sauvaud, N. Schneider, W. Sidney, S. Sparacino, A. I. Stewart, R. Tolson, D. Toublanc, C. Waters, T. Woods, R. Yelle, R. Zurek, The mars atmosphere and volatile evolution (MAVEN) mission, Space Science Reviews 195 (1-4) (2015) 3–48.

[13] D. C. Folta, Mars Atmosphere and Volatile Evolution (MAVEN) mission design, Advances in the Astronautical Sciences 136 (2010) 1401–1415.

[14] ESA, Mars Express - The Scientific Payload, no. 1240, 2004.

[15] D. Han, D. Highsmith, M. Jah, D. Craig, J. Border, P. Kroger, Mars Express interplanetary navigation from launch to Mars orbit insertion: The JPL experience, European Space Agency, (Special Publication) ESA SP (548) (2004) 195–200.

[16] NASA, 2001 Mars Odyssey (2001).

[17] R. Arvidson, W. V. Boynton, F. A. Cucinotta, M. Meyer, 2001 Mars Odyssey Mission Summary (January) (2004).

[18] L. Liberti, N. Maculan, A. Mucherino, C. Lavor, Euclidean Distance Geometry and Applications 56 (1) (2014) 3–69.

[19] G. A. Landis, Eccentricity and Inclination Reduction Following Capture on Martian Moons, 52nd Lunar and Planetary Science Conference 2021 (2021) 2–3.

[20] F. Pinto, SPAD files. Note 1 (Jupyter Notebook v. 1.0) (2023).
URL https://osf.io/tehp2/